The AFTA coronagraph instrument

Stuart Shaklan[1a], Marie Levine[a], Marc Foote[a], Michael Rodgers[b], Mike Underhill[a], Luis Marchen[a], Dan Klein[a]
[a]Jet Propulsion Laboratory, California Institute of Technology, 4800 Oak Grove Dr., Pasadena CA 91109;
[b]Synopsys, Inc, 3280 East Foothill Boulevard, Suite 300, Pasadena, CA 91107

ABSTRACT

The Astrophysics Focused Telescope Assets (AFTA) study in 2012-2013 included a high-contrast stellar coronagraph to complement the wide-field infrared survey (WFIRST) instrument. The idea of flying a coronagraph on this telescope was met with some skepticism because the AFTA pupil has a large central obscuration with six secondary mirror struts that impact the coronagraph sensitivity. However, several promising coronagraph concepts have emerged, and a corresponding initial instrument design has been completed. Requirements on the design include observations centered 0.6 deg off-axis, on-orbit robotic serviceability, operation in a geosynchronous orbit, and room-temperature operation (driven by the coronagraph's deformable mirrors). We describe the instrument performance requirements, the optical design, an observational scenario, and integration times for typical detection and characterization observations.

Keywords: Coronagraphy, external occulters, starshades, error budget, high contrast imaging

1. INTRODUCTION

NASA's Science Mission Directorate has begun the study phase of the WFIRST-AFTA mission,[1] with an anticipated launch date early in the next decade. The primary instrument is a wide-field infrared camera that will cover 0.28 sq. deg in a single image, an area 200 times larger than the Hubble Deep Field image, with a resolution of 0.11 arcsec. This camera will serve two main purposes: reveal the nature of dark energy by measuring accurate redshifts and the shapes of lensed galaxies; and search for exoplanets through observation of microlensing events. A high-contrast stellar coronagraph is also planned. This instrument will directly image and characterize Jupiter-mass planets around nearby stars and will image exozodiacal disks to within a few AU of the host star. The coronagraph is slated to observe for 1 year spread over the 6 year mission, but during this time the wide-field instrument will simultaneously observe fields of opportunity.

The mission will utilize a repurposed 2.4 m space flight-qualified telescope that is obscured by a ~30% central obstruction and 6 secondary support struts (figure 1). While this pupil considerably complicates the design of a high-contrast coronagraph, several promising approaches have emerged that are expected to enable detection of 10^{-9} contrast objects to within the 3rd Airy ring of the point spread function in broad-band light.[2-6]

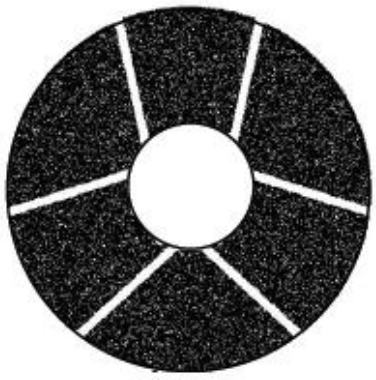

Figure 1: Approximate AFTA pupil with central obscuration and six secondary support struts.

The design reference mission places the telescope in an inclined geosynchronous orbit where future commercial robotic servicing capabilities may allow replacement/upgrade of the science instruments and key spacecraft components. For this reason, the instruments will be installed on a radial rail system within a multi-bay instrument carrier structure behind the primary mirror. A key area of ongoing study is the thermal stability of the coronagraph instrument in this orbit and integrated analysis of the optical train stability.

[1]Email: Stuart.b.shaklan@jpl.nasa.gov; Phone: 818-354-0105

Techniques and Instrumentation for Detection of Exoplanets VI, edited by Stuart Shaklan, Proc. of SPIE Vol. 8864, 886415 · © 2013 SPIE · CCC code: 0277-786X/13/$18 · doi: 10.1117/12.2024560

Notably, the coronagraph is slated to work at 290-300K (this is driven by wavefront requirements on the active deformable mirrors), while the wide-field IR instrument will be much colder, likely 220K. The instrument carrier will be at an intermediate temperature, and the telescope itself will operate at about 270K. Thermal control design is central to the success of the mission as both the wide-field and coronagraph instruments require pristine temperature stability.

The top-level coronagraph science objective from the WFIRST Science Definition Team report[1] is: *Directly image giant planets and debris disks from habitable zones to beyond the ice lines, around nearby AFGK stars, at visible wavelengths, and characterize their physical properties by measuring brightness, color, spectra, and polarization while providing information to constrain their orbital elements with an optional coronagraph.*

The report also includes a Science Objectives table with additional detail for coronagraph images scale, resolution, and bandpass:

- *Field of view from 0.1 – 1.5 arcsec at 400 nm, scaling linearly with wavelength up to 1000 nm (inner and outer radii of detection and characterization region)*
- *Allow for a survey of at least 150 stars with non-zero probability of detection*
- *Ability to image disks and map their structure with sub-AU angular resolution*
- *Single detection/characterization waveband of at least 10%*

2. INSTRUMENT CHARACTERISTICS

The coronagraph design parameters (Table 1) flow from the science objectives. The three most critical parameters in Table 1 are the inner working angle (IWA), the detection contrast limit, and the instrument contrast level. The IWA sets the minimum detection angle between the host star and planet. At 100 mas, the requirement is close to the third Airy ring (more precisely, an angle of 3 λ/D where λ is the minimum wavelength 400 nm and D = 2.4 m). At this close proximity to the core of the point spread function, the scattered light level is highly sensitive to minute changes in the system's low-order wavefront, and will require control of focus, astigmatism, coma, trefoil, and spherical aberration to levels of a few picometers during detection and characterization integrations.[7,8] It will be extremely challenging to reach the detection goal of 10^{-9} contrast at 100 mas for wavelengths greater than 500 nm (IWA < 2.4 λ/D). Thus the 400 – 500 nm band may serve as a planet discovery band while characterization across the full spectrum may be possible for planets at >200 mas separation from their host stars.

Table 1. Optical Parameters

Parameter	Value	Comment
Bandpass	400-1000 nm	Measured sequentially in nine 10.5% bands
Inner Working Angle	100 mas	at 400 nm, 3 λ/D driven by challenging pupil and low order aberration sensitivity
	250 mas	at 1 um
Outer Working Angle	1 arcsec	at 400 nm, limited by 64x64 DM
	2.5 arcsec	at 1 um
Detection Limit	Contrast =10^{-9}	Cold Jupiters, not exo-earths. Deeper contrast looks unlikely due to pupil shape and extreme stability requirements.
Instrument Background	Contrast = 10^{-9}	Q=1 for Instrument background relative to the detection limit. Important for stability requirements and integraton time.
Spectral Resolution	70	With IFS, ~70 across the spectrum.
IFS Spatial Sampling	17 mas	This is Nyquist for λ400 nm.

The detection limit is a contrast level of 10^{-9}, roughly the contrast of a Jupiter-twin seen at quadrature orbiting a solar-type star. Smaller planets can be seen at smaller orbits, *e.g.* a Neptune size planet at 2 AU has about the same contrast as a Jupiter at 5 AU. The detection limit requires instrument contrast calibration to ~ 2 x 10^{-10} for SNR=5 detection.

Instrument background, the average level of starlight leaking through to the image plane during an observation, is the third key parameter. A high background level increases Poisson noise and drives integration times. An instrument background scatter level of 10^{-9} (that is relative to the peak of the Airy pattern when a coronagraph is not present) scatters about 75% as much light as the combined solar system zodiacal light plus exozodiacal light from the target star assuming a similar particle density as the solar system. If the instrument contrast is allowed to rise to a level greater than 10^{-9}, then it will drive the integration times in proportion to the background level. It is also desirable to keep the instrument scatter low because it acts to 'heterodyne' any changes in the system wavefront that occur during observations and can greatly increase sensitivity to thermal drifts or other dynamic effects.[8] For example, a wavefront change that in the absence of any other scatter would cause a 10^{-10} contrast change would instead result in a $\sim 10^{-9}$ contrast change when mixed with instrument scatter of 10^{-8}. We have set the instrument scatter goal to be 10^{-9} because this is the best contrast so far obtained in calculations of scatter at 3 λ/D in 10% bandpass assuming the AFTA pupil.[2]

Table 2. Operational Characteristics

Coronagraph Type	Designed to support Lyot, Vector Vortex, PIAA and shaped pupil coronagraphs.
Operating Temperature	Room Temperature, due to DM wavefront specifications.
Deformable Mirrors	Two 64x64 devices, sequentially placed for broadband dark hole control. Current design is for Xinetics DMs with 1 mm pitch.
Detectors	Direct Imaging: 1K x 1K visible detector, 12 um (TBR) pixels Low Order Wavefront Sensor: E2V 39 (TBR), 24 um pixels IFS: 2K x 2K detector, ultra-low noise. 6.5 um pixels
IFS Bandpass	9 filters: 400-444 nm, 444-494 nm, 494-549 nm, 549-610 nm, 610-678 nm, 678-753 nm, 753-836 nm, 836-929 nm, 928-1032 nm

Exoplanet spectra will be characterized with a low resolution spectrometer. Following the TPF-C requirements,[9] a spectral resolution of 70 is selected to resolve the O_2 line at 0.76 um.[10] The spectral characterization will be carried out with an Integral Field Spectrometer (IFS, described below) that will spectrally resolve each pixel in the dark hole. A pixel size of 17 milli-arcsec is required to Nyquist sample the image at the minimum wavelength of 400 nm.

Table 2 lists the key coronagraph operational characteristics. At the present time five candidate coronagraph approaches are being studied for use in the mission. The coronagraph layout discussed below, can, with minor modifications, support all but the visible nulling coronagraph (VNC) [6] which has a two-stage shearing nuller, a segmented deformable mirror, and a spatial filter array consisting of lenslets and single mode fiber optics or an integrated optics array.[11]

The Lyot, Vector Vortex, PIAA, and shaped pupil coronagraphs use continuous face sheet deformable mirrors (DMs). These are available in formats up to 64x64 pixels. Both Xinetics DMs, with a 1 mm pitch,[12] and Boston Micromachines (BMC) DMs with a 300 um pitch,[13] are candidates for the flight instrument. They both have ~1 um surface deformation range and are driven by 100-200 V multiplexed power supplies. The Xinetics devices have been used in the JPL High Contrast Imaging Testbed (HCIT)[14] to obtain broad-band contrasts of better than 10^{-9}, while the BMC devices are in employed in high contrast testbeds at Ames, Princeton, and U. Hawaii. Both the Xinetics and BMC DMs are designed to work at room temperature and will have reduced correctability at other temperatures.

The instrument includes three detectors: direct imaging, spectral-imaging, and a low-order wavefront sensor (LOWFS). The direct imaging channel has higher throughput than the IFS and may prove to be the more effective discovery channel. Though the coronagraph dark hole will only be up to 2.5 arcsec wide, we have sized the detector to be 1K x 1K pixels providing a 17 arcsecond field for imaging of disks. The 2K x 2K IFS detector is sized to provide SR=70 spectroscopy over 140 x 140 lenslets, each subtending 17 mas, in a 10.5% bandpass. Details on this scaling are provided in Section 3. Both of these detectors are photon-counting devices with extremely low read noise. Finally, the LOWFS detector is a small format device used to measure low-order aberrations in a to-be-designed sensor. The sensor will

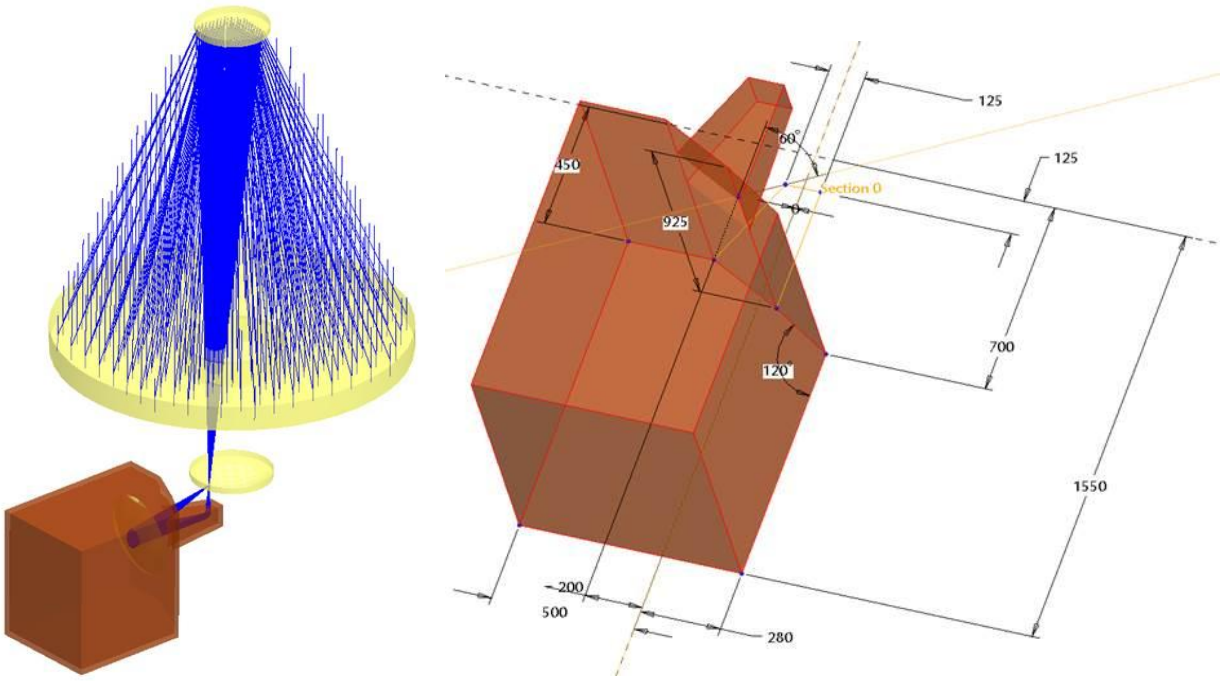

Figure 2. The box shows the coronagraph volume. The small disk behind the primary mirror indicates a 0.6 deg radius in the Cassegrain image plane.

either use reflected light from around the core of the coronagraph mask,[15] or an interferometric approach using a reference beam in a similar fashion to the self-coherent camera.[16,17]

Ideally the coronagraph would collect all of the light over the 400-1000 nm bandpass in one image. Unfortunately, the useful bandpass for wavefront correction for AFTA coronagraphs is likely to be ~10% because the architectures use combinations of complex amplitude masks, pupil apodizers, and wavefront control to suppress diffraction from the obscured pupil. We have thus included filters that pass 10.5% bands as detailed in Table 2. Additionally, to keep the detector size to 2Kx2K and to isolate the spectra transmitted by each lenslet, the IFS is designed to work over any 18% band between 400-1000 nm.

3. INSTRUMENT DESIGN

A volume approximately 1.1 x 0.8 x 0.93 m^3 has been allocated for the AFTA coronagraph (figure 2). The flat mirror mounted at the end of the snout (figure 3) serves to transfer the beam into the main body while avoiding interference with the surrounding wide-field instrument and fine guiding fields of regard. There is a single-use shutter (not shown) located above the pickoff mirror that keeps the coronagraph clean prior to on-orbit observations. The portion of the coronagraph optical train between the pickoff mirror and the Lyot stop must be maintained at a cleanliness level of CL100 to ensure that instrument scatter is well below the exozodiacal background light level.[18] Because the image plane mask removes most of the starlight, cleanliness of downstream optics is not as critical.

We discuss two optical configurations. The first is the simplest form of Lyot coronagraph, with a minimum number of pupil and image planes. This configuration can be used with the Lyot, vector vortex, and potentially with the shaped pupil coronagraph (SP), though the SP would have to be placed either on a DM or in the beam between DMs. The design does not have a second image plane where a field stop can be placed to block the bright light from around the dark hole. The second configuration adds two reflections and provides more versatility, including accommodation for a PIAA coronagraph, albeit with slightly increased loss and degraded wavefront due to the additional optics.

3.1 Barebones Configuration

The pickoff mirror reflects the light to the tertiary mirror, a conic that corrects the off-axis aberrations. Light is reflected to an off-axis parabola (OAP) that forms a pupil image at the first DM (DM1). The DMs shown here are 64x64 mm Xinetics devices with a 1 mm pitch. The baseline design may change to a 48 mm beam but the layout is similar. DM1 is mounted on a tip-tilt stage to provide pointing control. It is followed by a flat and then the second DM (DM2), one meter downstream from DM1. The combination of DMs allows both phase and amplitude control; amplitude is controlled via propagation of light from DM2 to the pupil and is wavelength-independent by virtue of the cancellation of λ-dependent propagation with 1/λ-dependent DM phase.[19]

After DM2, the light is focused at f/25 by an OAP. Figure 3 indicates the focus/occulter image plane where the coronagraph mask is installed for a Lyot or vector vortex design. For a hybrid band-limited coronagraph, this plane provides the LOWFS signal using the light rejected by the mask. For a vector vortex, the LOWFS signal is derived from the light diffracted around the Lyot plane. The Lyot plane is then formed in the collimated space between two OAPs. Diffracted starlight is stripped off by the Lyot mask and the remaining leaked starlight and planet light are filtered through either narrow band filters (likely 2% wide as in HCIT) for wavefront sensing, or a 10.5% filter for imaging and

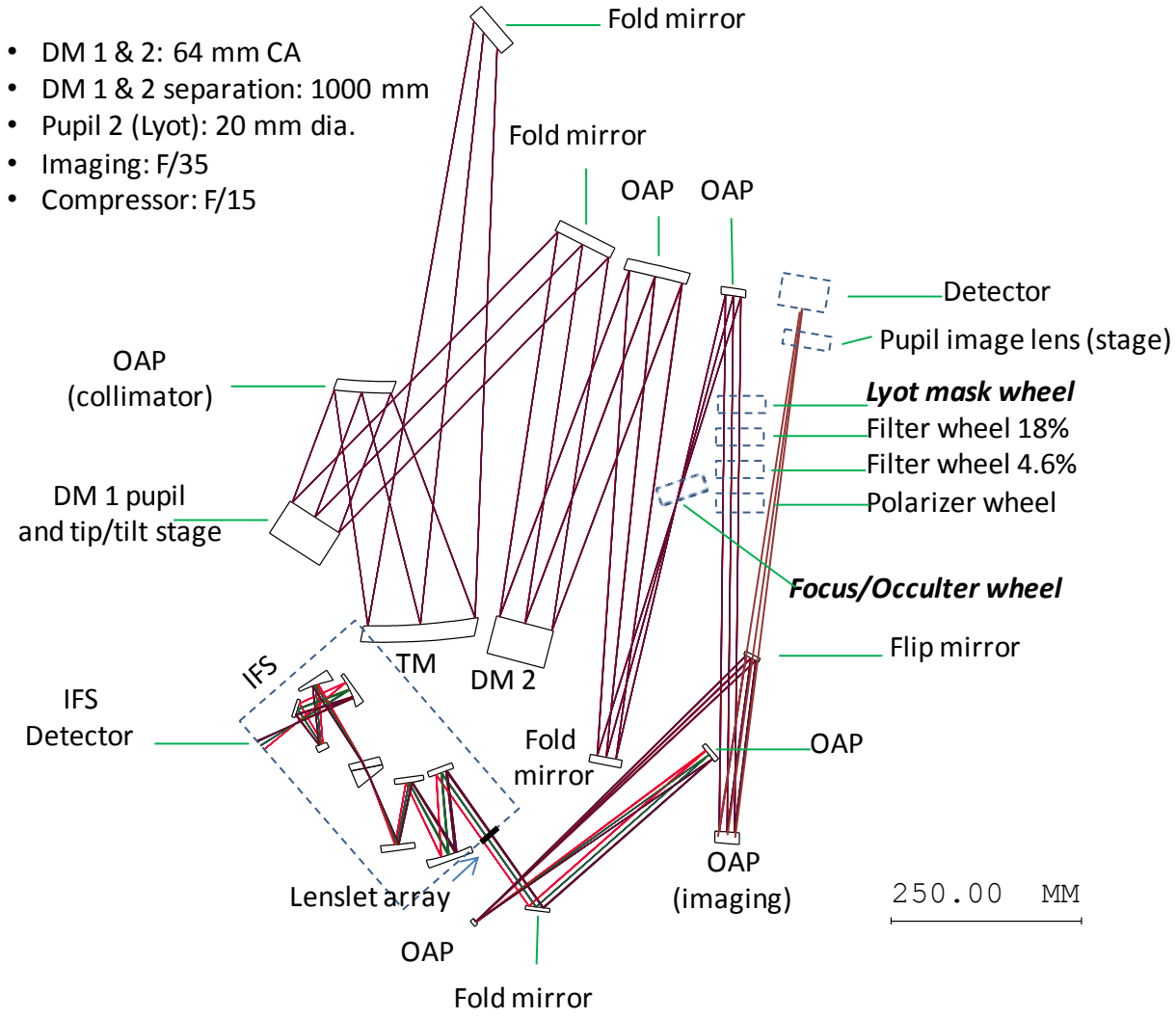

Figure 3. The coronagraph layout is for a pair of 64 x 64 mm DMs separated by 1 m of optical path. This design has only one occulter plane and one plane for a Lyot stop. It may be possible to accommodate a reflective pupil mask at the flat between the two DMs.

spectral characterization. Polarizers may also be placed in the beam for polarization studies of scattered planet and stellar disk light.

The final OAP directs the beam to either the direct imaging camera, or to a flip-in mirror that reflects the light into the IFS. As noted above, the 1k x 1k direct imaging camera has a 17 arcsec wide field. It also works in conjunction with a pupil-imaging lens on a 2-axis stage that can be inserted and adjusted to form defocused images of the pupil. These focus diversity images are used to estimate the nominal wavefront so that the coronagraph high-contrast wavefront control loop can begin with a flat (to a few nm) wavefront.

The IFS arm comprises a beam expander to match the pupil image to the 100 um pitch, 140x140 lenslet array. Each lenslet design is actually an air-spaced doublet, with a field lenslet followed by a focusing/telecentric lenslet. This is similar in concept to the SPHERE IFS[20] but without the micro-pupil array. Each lenslet samples a 17 milli-arcsec region of the image plane so that the full field of the IFS camera is 2.4 arcsec. A 4-element collimator transfers the pupil image from the lenslets to the 65 mm diameter plane where the dual-element dispersing prism is placed. This prism gives approximately constant dispersion over the 400-1000 nm bandpass. Following the prism, a compact folded 4-element camera images the dispersed 'spaxels' onto a 2k x 2k format ultra-low noise detector with a 6.5 micron pitch. The illuminated area is 13.9 mm, providing about 15 pixels between spaxels. An 18% wide spectrum is dispersed over 26 pixels or 0.17 mm.

Figure 4 shows the optics placed on a stiff, athermalized, planar optical bench within the allocated volume. The figure also shows an electronics box and a volume set aside for the low-order wavefront sensor. There is substantial room to fold the instrument out of plane, but this does not relieve the tight-fit of the first 4 optics following the fold mirror.

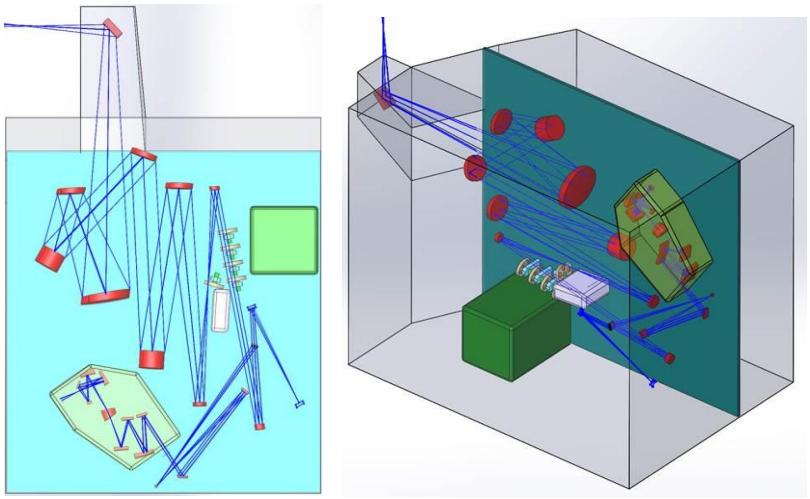

Figure 4. The instrument is shown packaged in the allocated volume. The green box represents the electronics package.

3.2 Versatile Configuration

By adding two OAPs in the system, an additional pupil and image plane are formed (figure 5). This provides versatility for placing a field stop at the second focus, and an apodizer for the VVC at the intermediate pupil. Further, by replacing the two OAPs following DM2 with PIAA optics, the system can be used in a PIAA configuration as well. One further modification is considered for the Shaped Pupil coronagraph configuration. Shaped pupils for the obscured AFTA pupil contain 'islands' of dark and transparent regions that cannot be made self-supporting in a machined part.[5] The pupils can be made using photolithography on a glass substrate but this is undesirable due to the transmission non-uniformities in the glass (any dispersion must be corrected by the DMs and will limit performance). Another possibility is to manufacture the masks using 'black silicon'[21], etching, leaving a highly absorptive region interspersed with a high-quality silicon mirror. This reflective pupil mask could be placed at the location of the pupil plane shown at the bottom of figure 5, folding the beam (and the rest of the optical train) at that location.

4. CORONAGRAPH IMPLEMENTATION

High contrast coronagraphy requires extreme stability of the optical system over the observation time period. For any of the possible coronagraph options, AFTA coronagraph optics require ~0.25 μm relative stability during an observation. The coronagraph optical bench must be positioned to within 0.5 mm with respect to the telescope, and this relative position must be stable to 0.25 mm during an observation period. The optical bench is thermally stabilized to <10 mK to achieve 0.25 μm internal stability. Three latches on the back of the

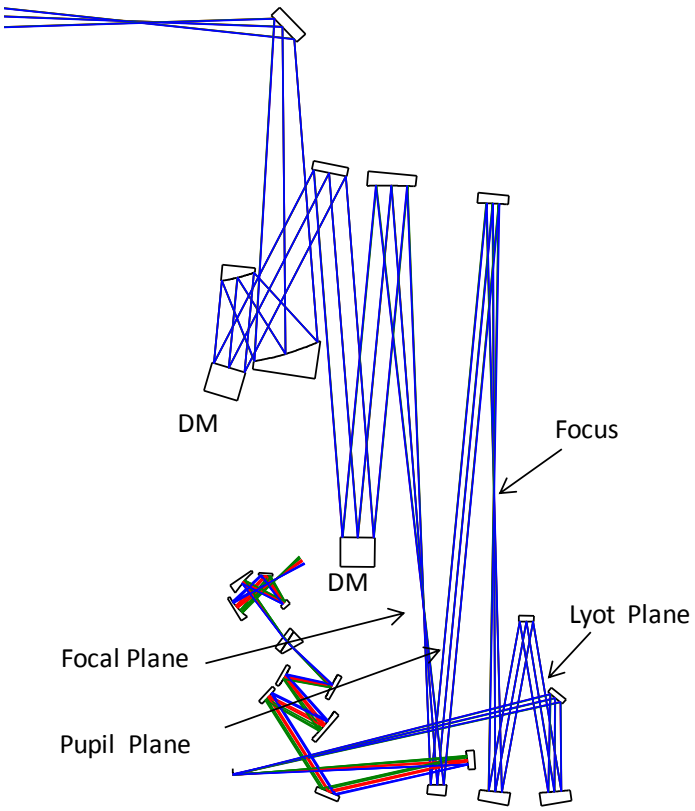

Figure 5. One additional reflection upstream of the occulter and another before the Lyot stop provide a focus following the a pupil plane. The focus can be used as a field stop to block light outside the dark hole, and it can be used as the occulter plane for a PIAA or shaped pupil coroangraph.

optical bench will secure the coronagraph to the instrument carrier. The instrument carrier must be thermally stable enough to support the required dimensional stability, and a metrology and fine positioning system may be needed.

The coronagraph optical bench assembly is maintained at 290 K to ensure that the DMs are flat when unpowered. The LOWFS detector is cooled to ≈250 K with a Peltier cooler while the coronagraph imaging detector and IFS detector are cooled to ≈150 K by radiators to minimize dark current. Thermal isolation is provided at the three mechanical contacts to the instrument carrier (latches). Blanketing isolates the coronagraph radiatively from the 220 K instrument carrier. Coronagraph temperature is maintained with its electronics power dissipation in addition to software-controlled heaters.

The coronagraph image plane and IFS detectors must have extremely low noise. Dark current noise must be no more than 1 e- over a thousand to several thousand seconds, while read noise must be no more than 1 e- for the sum of 100-1000 reads. Silicon detectors can provide this low dark-current noise when cooled to ≈150K. Very low read noise is more difficult to obtain. Two detector options are under consideration. The e2v electron-multiplying charge-coupled devices (EMCCDs) have demonstrated the required read noise. 1k x 1k devices are already commercially available, and 4k x 4k devices should be available by 2014 or 2015. However, radiation damage can increase the read noise considerably. Work is needed to determine whether proper operating conditions can mitigate the radiation-induced read noise. A second promising technology is Geiger-mode avalanche photodiodes, being developed by the University of Rochester and MIT Lincoln Laboratories. Further work will be needed to demonstrate arrays with adequate performance and array size.

5. INTEGRATION TIMES

The AFTA coronagraph will be able to detect the presence of Jupiter analogs with a few hours of integration time. Table 3 shows the integration time for both Jupiter and Earth analogs orbiting a star with visual magnitude V=5, two levels of instrument contrast, and a range of detector dark current and read noise. The table assumes that the combined background and planet photometric noise is 5 times lower than the planet signal, or photometric SNR=5. A more rigorous calibration requirement is set by the desired false alarm probability and the probability of missed detection.[22]

Table 3 shows that without read noise or dark current noise, the integration time for a Jupiter analog around a V=5 star, with an instrument background of 10^{-9} contrast, is about 1.4 hours. This increases substantially to 4.8 hours when the

instrument background is 10^{-8}. As noted earlier, not only does the instrument background increase integration times, it also increases sensitivity to wavefront errors. Thus instrument background has a strong influence on the stability time constant of the system. Detector noise plays an important role in the imaging channel. Table 3 shows that dark currents of 0.001 e-/s and read noise of 0.5 e-/pixel cause the integration time to double to 2.7 hours, while 1 e- read noise increases integration time to 5.4 hours. These results assume that the detector is read out every 100 s to assist in the rejection of cosmic rays.

Table 3. Integration time for detection

AFTA Integration Time Examples, 10% bandpass

For V=5, Exozodi density = solar system, 100 s readout, 10% bandpass, Coro throughput 0.2, Telescope throughput 0.6

log10(Planet Contrast)	log10(Instr. Contrast)	Dark current (e-/pix/s), Read Noise e/pix	INTEG. TIME (Hours)	Comment
-9	-9	0 , 0	1.37	Jupiter, Noiseless detector
-9	-9	0, **0.1**	1.41	Read noise
-9	-9	0, **0.2**	1.52	More read noise
-9	-9	0, **0.5**	2.29	More read noise
-9	-9	**0.0001**, 0	1.41	Dark Current
-9	-9	**0.0002**, 0	1.45	More dark Current
-9	-9	**0.001,** 0	1.74	More dark current
-9	**-8**	0, 0	4.8	Instrument-limited
-9	**-8**	0.001, 1	8.4	Instrument-limited
-10	-9	0.0001, 0.1	111	exo-Earth
-9	-9	**0.001/0.5**	2.7	Jupiter, RN and DC
-9	-9	**0.001/1**	5.4	more RN and DC

Table 4. Integration time for characterization

AFTA Integration Time Examples, 2% bandpass

For V=5, Exozodi density = solar system, 100 s readout, 2% bandpass, Coro throughput 0.2, Telescope throughput 0.6, IFS throughput =0.5

log10(Planet Contrast)	log10(Instr. Contrast)	Dark current (e-/pix/s), Read Noise e/pix	INTEG. TIME (Hours)	Comment
-9	-9	0 , 0	13.7	Jupiter, Noiseless detector
-9	-9	0, **0.02**	13.9	Read noise
-9	-9	0, **0.05**	14.6	More read noise
-9	-9	0, **0.1**	17.4	More read noise
-9	-9	**0.00005**, 0	15.6	Dark Current
-9	-9	**0.0001**, 0	17.4	More dark Current
-9	-9	**0.001,** 0	50	More dark current
-9	**-8**	0, 0	47	Instrument-limited
-9	**-8**	**0.0001/0.1**	55	Instrument-limited
-10	-9	0.0001, 0.1	1770	exo-Earth
-9	-9	**0.0001/0.1**	21	Jupiter, RN and DC
-9	-9	**0.001/0.5**	142	more RN and DC

Detection of exo-earths appears to be extremely challenging for the system. Even at extremely low levels of read noise and dark current, and with instrument background clamped at 10-9, the integration time for an earth-analog is 111 hours.

Spectral characterization times (table 4) are ~10x longer because the spectral bandwidth is narrower (from 10% to 2%), and the instrument throughput is reduced (by a factor of 2). Detector noise is more critical in the IFS, as even dark

current of 0.0001 e-/s and read noise of 0.1 e- increase integration time from 14 hours to 21 hours for Jupiter-analog characterization. Increasing the instrument background to 10^{-8} drives the characterization time to 55 hours.

The integration time for control of the dark hole is key parameter that drives the stability requirements and the available time for science integrations. When instrument background light, exozodiacal light, and detector noise are present, the integration time for controlling speckles at a given contrast level is the same as for detecting a planet; both are limited by the same photometric noise. However, it is possible to take the bright light that is rejected by the coronagraph and interfere it with the light leaked by the instrument (e.g. refs. 15,16). The interference term can be much brighter than the background and its calibration will be limited only by the Poisson noise in the leakage term, rendering the zodiacal light and detector noise moot. This fundamental integration time is 3.7 hours under the following assumptions: speckle contrast = 10^{-9} detected with SNR=5; there is no other background or photometric noise; 10% bandpass measured in the IFS because 2% spectral resolution is required to control the wavefront across the 10% band; V=5 star. For a coronagraph with 20% throughput, this is the shortest time in which one can measure the instrument background and sets the minimum instrument stability time for maintaining contrast sufficient to detect planets having 10^{-9} contrast. One must also account for the gain of the control system in computing the minimum stability time. Groff et al provide a similar argument and calculation and examples of control loops operating to maintain contrast.[23]

6. CONCLUSION

We have introduced the AFTA coronagraph instrument without describing the diffraction control system! At the time of writing, the candidate coronagraphs along with the visible nullers are being evaluated through modeling and other criteria (e.g. complexity, sensitivity to perturbations, maturity, mass, power….) The downselect to two concepts is expected to happen in the spring of 2014 with the selection of a primary and backup approach. Meanwhile, we have explored the implementation of the various concepts and found, not surprisingly, that their optical trains are similar in many respects, and that all will fit within the allocated volume. In this paper we have shown a baseline coronagraph implementation and a slightly more complex and versatile one that will accommodate hybrid band-limited, vector vortex, shaped pupil, and PIAA coronagraphs.

The AFTA coronagraph will be powerful enough to characterize Jupiter analogs around nearby bright stars. We have shown one possible approach to characterization based on an integral field spectrometer. Other approaches include dichroic trees, fiber-fed spectrometers, and single-reflection high-efficiency slit grating spectrometers.

We would like to acknowledge many useful conversations and technical exchanges with David Content, Kevin Grady, Mark Melton, and the WFIRST team at Goddard Space Flight Center. This work was carried out at the Jet Propulsion Laboratory, California Institute of Technology, under contract to the National Aeronautics and Space Administration.

REFERENCES

[1] D. Spergel *et al*, Wide-Field Infrared Survey Telescope-Astrophysics Focused Telescope Assets WFIRST-AFTA Final Report, http://wfirst.gsfc.nasa.gov/science/sdt_public/WFIRST-AFTA_SDT_Final_Report_Rev1_130523.pdf (2013)

[2] J. Trauger *et al*, "Complex apodized Lyot coronagraph for exoplanet imaging with partially obscured telescope aperture," Proc. SPIE 8864 (2013).

[3] O. Guyon, "Imaging Earth-like planets around late-type stars with low-inner working angle PIAA coronagraphy," Proc. SPIE 8864 (2013).

[4] D. Mawet *et al*, "The ring-apodized and multistage vortex coronagraph: two simple, small-angle coronagraphic solutions for heavily obscured apertures," Proc. SPIE 8864 (2013).

[5] A. Carlotti, N. J. Kasdin, & R. J. Vanderbei, "Shaped pupil coronagraphy with the AFTA telescope," Proc. SPIE 8864 (2013).

[6] R. Lyon et al, "High-contrast vacuum nuller testbed (VNT) contrast, performance, and null control," Proc. SPIE 8442, 844208 (2012).

[7] Shaklan, S. B., *et al.*, "The Terrestrial Planet Finder Coronagraph Dynamics Error Budget," Proc. SPIE 5905, 59050D-1 (2005).

[8] S. B. Shaklan *et al*, "Stability error budget for an aggressive coronagraph on a 3.8 m telescope," Proc. SPIE 8151, 815109 (2011).
[9] Levine, M., Shaklan, S. B., & Kasting, J., eds, "Terrestrial Planet Finder Coronagraph, Science and Technology Definition Team (STDT) Report," JPL Document D-34923, available at http://planetquest.jpl.nasa.gov/TPF/STDT_Report_Final_Ex2FF86A.pdf (2006).
[10] D. DesMarais *et al*, "Remote sensing of planetary properties and biosignatures on extrasolar terrestrial planets," Astrobiology 2, 153-181 (2002).
[11] J. Ai *et al*, "Planar waveguide integrated spatial filter array," Proc. SPIE 8864 (2013).
[12] J. Trauger et al, "A hybrid Lyot coronagraph for the direct imaging and spectroscopy of exoplanet systems: recent results and prospects," Proc. SPIE 8151, 8151OG (2011).
[13] S. A. Cornelissen, T. G. Bifano, & P. A. Bierden, "MEMS deformable mirror actuators with enhanced reliability," Proc. SPIE 8253, 825306 (2012).
[14] E. Sidick *et al*, "HCIT contrast performance sensitivity studies: simulation versus experiment," Proc. SPIE 8864 (2013).
[15] Guyon, O., Matsuo, T., & Angel, R., "Coronagraphic low-order wave-front sensor: principle and application to a phase-induced amplitude coronagraph," Ap. J., 693, 75-84 (2009).
[16] R. Galicher *et al*, "Self-coherent camera as a focal plane wavefront sensor: simulations," A&A 509, A31 (2010).
[17] A. Give'on *et al*, "Electric field reconstruction in the image plane of a high-contrast coronagraph using a set of pinholes around the Lyot plane," Proc. SPIE 8442, 84420B (2012).
[18] K. Balasubramanian, S. Shaklan, & A. Give'on, "Stellar coronagraph performance impact due to particulate contamination and scatter," Proc. SPIE 7440, 74400T (2009).
[19] S. B. Shaklan & J. J. Green, "Reflectivity and optical surface height requirements in a broadband coronagraph. 1. Contrast floor due to controllable spatial frequencies," Appl. Opt 45, 5143-5153 (2006).
[20] J. Antichi *et al*, "SPHERE IFS optical concept description and design overview," Proc. SPIE Vol. 7014, 7143H (2008).
[21] H.M. Branz *et al*, "Nanostructured black silicon and the optical reflectance of graded-density surfaces," Appl. Phys. Lett., 94, 231121-3 (2009).
[22] N. J. Kasdin, I. Braems, "Linear and Bayesian Planet Detection Algorithms for the Terrestrial Planet Finder," Ap. J. 646, 1260-1274 (2006). Erratum: Ap. J. 672, 734K (2008).
[23] T. Groff *et al*, "Wavefront control scenarios for a coronagraph on the AFTA space telescope," Proc. SPIE 8864 (2013).